United Time-Frequency Spectroscopy for Dynamics and Global Structure

Adela Marian, Matthew C. Stowe, John R. Lawall,* Daniel Felinto,† Jun Ye‡

Ultrashort laser pulses have thus far been used in two distinct modes. In the time domain, the pulses have allowed probing and manipulation of dynamics on a subpicosecond time scale. More recently, phase stabilization has produced optical frequency combs with absolute frequency reference across a broad bandwidth. Here we combine these two applications in a spectroscopic study of rubidium atoms. A wide-bandwidth, phase-stabilized femtosecond laser is used to monitor the real-time dynamic evolution of population transfer. Coherent pulse accumulation and quantum interference effects are observed and well modeled by theory. At the same time, the narrow linewidth of individual comb lines permits a precise and efficient determination of the global energy-level structure, providing a direct connection among the optical, terahertz, and radio-frequency domains. The mechanical action of the optical frequency comb on the atomic sample is explored and controlled, leading to precision spectroscopy with an appreciable reduction in systematic errors.

Ultrashort laser pulses have given a remarkably detailed picture of photophysical dynamics. In studies of alkali atoms (*1*) and diatomics (*2*) in particular, coherent wave packet motion has been observed and even actively controlled. However, the broad bandwidth of these pulses has prevented a simultaneous high-precision measurement of state energies. At the expense of losing any direct observation or control of coherent dynamics, precision spectroscopy enabled by continuous wave (cw) lasers has been one of the most important fields of modern scientific research, providing the experimental underpinning of quantum mechanics and quantum electrodynamics.

This trade-off between the time and frequency domains might seem fundamental, but in fact it results from pulse-to-pulse phase fluctuations in laser operation. The recent introduction of phase-stabilized, wide-bandwidth frequency combs based on mode-locked femtosecond lasers has provided a direct connection between these two domains (*3*, *4*). Many laboratories have constructed frequency combs that establish optical frequency markers directly linked to a microwave or optical standard, covering a variety of spectral intervals. Atomic and molecular structural information can now be probed over a broad spectral range, with vastly improved measurement precision and accuracy enabled by this absolute frequency-based approach (*5*). One of the direct applications is the development of optical atomic clocks (*6*–*8*). To date, however, traditional cw laser-based spectroscopic approaches have been essential to all of these experiments, with frequency combs serving only as reference rulers (*9*).

Here we take advantage of the phase-stable femtosecond pulse train to bridge the fields of high-resolution spectroscopy and ultrafast dynamics. This approach of direct frequency comb spectroscopy (DFCS) uses light from a comb of appropriate structure to directly interrogate a multitude of atomic levels and to study time-dependent quantum coherence. DFCS allows time-resolved studies of coherent and incoherent dynamics: We demonstrate coherent pulse accumulation, quantum interference, and global incoherent optical pumping. At the same time, DFCS exploits massively parallel spectral probing in the frequency domain with a comb bandwidth spanning tens to hundreds of terahertz (*10*), providing a systematic-free connection among various spectroscopic windows of interest. The optical coherence of a phase-stabilized pulse train provides a spectral resolving power approaching that of state-of-the-art cw lasers.

Two-photon DFCS. Our experimental prototype system to study DFCS is a set of two-photon transitions from the ground-state $5S_{1/2}$ to the excited $5D_{3/2}$ and $5D_{5/2}$ states in laser-cooled ^{87}Rb atoms (Fig. 1). The dipole-allowed intermediate states, $5P_{3/2}$ and $5P_{1/2}$, are located ~2 and 17 nm below the energy-degenerate virtual level for the two-photon transition, respectively. The lifetime of the 5P intermediate states is 27 ns, and the lifetime of the 5D states is 240 ns. Also shown (not to scale) is a regularly spaced comb of optical frequencies corresponding to that of the laser. The bandwidth associated with the femtosecond pulse is sufficiently broad that many fine and hyperfine atomic states can be excited by tuning the relevant comb components into resonance. Thus, one laser is used to measure the global energy-level structure while monitoring real-time transition dynamics of the atomic system.

The optical frequency of a particular comb mode can be expressed as $\nu_n = nf_r + f_0$, where f_r is the pulse repetition rate, f_0 is the carrier-envelope offset frequency, and n is an integer on the order of 10^6. Radio-frequency oscillators with ultralow phase noise or ultrastable lasers are used to control the optical comb (*11*). The sum frequency of the light from two comb lines labeled by m and n is given by $\nu_{2\gamma} = (m + n)f_r + 2f_0$. There are several hundred thousand comb pairs (m, n) that yield the same sum frequency and thus could contribute to the transition amplitude when $\nu_{2\gamma}$ is resonant with the two-photon transition ($\delta_{SD} \sim 0$ as shown in Fig. 1). However, it is necessary to consider the intermediate 5P states that provide resonant enhancement. When one of the comb lines is tuned near resonance with one of the 5S-5P transitions ($\delta_{SP} \sim 0$ as shown in Fig. 1), the resonant enhancement causes the corresponding pair to make the dominant contribution to the two-photon transition over all of the other pairs. The dominance is reinforced by destructive quantum interference between comb pairs symmetrically detuned on either side of the P state, resulting in a ~180° phase difference (*12*). For the nonresonant configuration of comb modes detuned $\pm kf_r/2$ ($k \geq 1$, odd integer) away from the P state, with all pairs satisfying the two-photon resonance, the transition amplitudes associated with ($+k$) and ($-k$) modes will again destructively interfere. However, there will be a net nonresonant contribution due mainly to the existence of multiple P states that break the symmetry of the comb distribution. This destructive interference can be made construc-

JILA, National Institute of Standards and Technology and University of Colorado Department of Physics, University of Colorado, Boulder, CO 80309–0440, USA.

*Permanent address: Atomic Physics Division, Mail Stop 8423, National Institute of Standards and Technology, 100 Bureau Drive, Gaithersburg, MD 20899, USA.

†Present address: Norman Bridge Laboratory of Physics, 12-33, Caltech, Pasadena, CA 91125, USA.

‡To whom correspondence should be addressed. E-mail: ye@jila.colorado.edu

tive by flipping the spectral phase about the P state (*12*). Given the two degrees of freedom associated with f_r and f_0, it is always possible to tune a comb to satisfy the two-photon as well as single-photon resonance with any desired intermediate P state. Phase coherence among transition pathways excited by different combinations of comb modes can cause multipath quantum interference effects on the transition probability. The two-photon transition spectrum is obtained by scanning f_r or f_0; their precisely known values, along with (m, n), determine all relevant atomic energy levels in absolute terms.

Traditionally, Doppler-free two-photon spectroscopy has been carried out with two equal-frequency cw laser beams propagating in opposite directions. The two-photon transition rate was resonantly enhanced via available intermediate states using either two different excitation laser frequencies (*13*) or high-velocity atomic beams (*14*). High-resolution two-photon spectroscopy using picosecond pulsed light, hence without any appreciable intermediate-state interaction or absolute frequency reference, has been previously demonstrated (*15*, *16*).

The preceding discussion in the frequency domain, based on an interpretation of the laser spectrum as a set of discrete lines, is complemented by the time-domain multipulse interaction picture (Fig. 1). The pulse-to-pulse optical coherence gives the spectrum its discrete nature, and the time over which optical coherence is maintained determines the width of each line in the comb. The relevant laser parameters for describing the interaction are the interpulse period $\tau = 1/f_r$, the carrier envelope phase evolution between successive pulses $\Delta\phi$, and the pulse duration and its associated area. For times that are short compared to the atomic decoherence time, the femtosecond pulse train drives the atomic coherence in phase such that a multipulse excitation is coherently built up for resonant atomic states. At longer times, however, the coherence in the optical field can no longer be transferred to the atom owing to the finite atomic coherence time. Incoherent processes such as optical pumping then govern the population transfer dynamics. This multipulse interference, combined with a large pulse bandwidth, gives an interesting variation and generalization of the traditional Ramsey technique.

Modeling coherent interactions. The interaction of the femtosecond comb with the atoms was modeled via the Liouville equation for the density matrix of all the atomic states in the laser bandwidth accessible through two-photon absorption, with radiative relaxation included via phenomenological decay terms. The density matrix equations were solved using a perturbative expansion in the field to fourth order. With the approximation of impulsive optical excitation during the pulse, followed by free evolution and decay, an iterative procedure was used to determine the state of the atomic system after any number of pulses (*17*, *18*). The model includes the fine and hyperfine structure of the 5S, 5P, and 5D states, with the Zeeman substructure averaged for linear polarization. A theoretical transition spectrum was constructed with energy-level information provided by the literature, against which we present a comparison with our own measurements. In the simulation, we used calculated oscillator strengths and Clebsch-Gordan coefficients for all involved transition pathways in an effort to accurately predict the relative signal strengths. This general set of Bloch-type equations, evolving from one pulse to the next, leads to a global picture of coherent population accumulation and incoherent optical pumping.

Temporal coherent control is best manifested in the 5D coherent population accumulation and transition linewidth evolution, which through the coherent interaction with the train of femtosecond pulses reach their asymptotic limits imposed by the atomic decoherence. The model results (Fig. 2), under the condition of a small pulse area, illustrate the effect of pulse accumulation on signal strength and spectral linewidth. The on-resonance 5D population increases as the square of the number of pulses until reaching approximately the decoherence time, 480 ns for the 5D states (Fig. 2A). This rapid population increase is accompanied by the narrowing of the resolution linewidth (Fig. 2B), analogous to the spatial resolution and power density scaling versus the number of slits in a multislit experiment. Experimentally we have verified both aspects of this coherent pulse accumulation effect. The effect of the quadratic increase of the excited-state population versus the accumulated number of pulses can be further enhanced with a larger f_r. At long time scales, the global incoherent population transfer has been observed to obey the model prediction.

Experimental method. The experiment was performed with an optical frequency comb (emitted from a 20-fs, 100-MHz repetition rate, mode-locked Ti:sapphire laser) centered at 780 nm with a full width at half maximum bandwidth of ~55 nm (~26 THz). There is ~200 nW of power in the comb lines resonant with the 5S-5P and 5P-5D transitions. The light was typically focused to a beam waist of 130 μm, giving an on-axis intensity of ~0.8 mW/cm^2 in each comb line. For time-resolved studies, the sample was exposed to light by a liquid crystal shutter with a 30-μs response time.

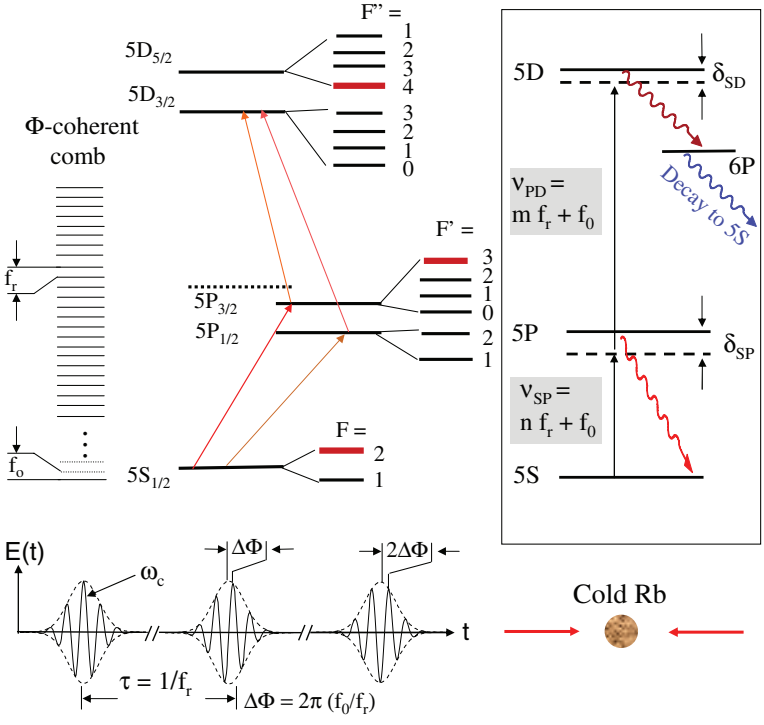

Fig. 1. (**Top**) Schematic of the ^{87}Rb energy levels participating in the 5S-5D two-photon transitions, and the frequency-domain perspective of the atom-light interaction. (**Bottom**) Time-domain picture showing a sequence of mode-locked pulses, with the important interaction parameters τ and $\Delta\phi$. The inset at right shows the relevant "three-level" model used for construction of the Bloch equations to solve for population transfer dynamics. In particular, we show an example of the resonantly enhanced transition with detunings δ_{SP} and δ_{SD} for the pair of comb modes that makes the dominant contribution to the transition probability.

The atomic source was a cloud of ^{87}Rb trapped and cooled in a vapor-cell magneto optical trap (MOT). To minimize magnetic fields during data acquisition, we extinguished the trapping quadrupole magnetic field 2 ms before application of the light from the frequency comb and held the atoms in optical molasses (~20 μK) during this time. The residual magnetic field was compensated by nulling the Zeeman frequency shifts of the two-photon transitions in all three directions using three pairs of bias coils. We extinguished the molasses beams before applying the comb light.

A cw repumping laser controlled the initial populations of the two ground-state hyperfine levels. During the actual probing period, the femtosecond comb itself acts as a repumper, allowing one to maintain a stable population in the initial ground state. The population in the 5D state decays to the 6P state, and the subsequent fluorescent decay at 420 nm from 6P to 5S was detected with a photomultiplier, used in photon counting mode. The counts were then binned on a multichannel analyzer with a typical integration time of 10 μs, and this signal was averaged over hundreds of 20-ms MOT cycles.

Scanning f_r gives a full spectrum. Figure 3 shows the two-photon transition spectrum obtained by scanning f_r for a fixed value of f_0 using linearly polarized light. Also shown is the corresponding theoretical spectrum for the set of parameters used in the experiment. The two insets show signal magnitude on a logarithmic scale to enhance the visibility of the smaller peaks. A total of 39 pathways and 14 transitions have been identified for the $5S_{1/2} \rightarrow 5D_{3/2}$ and $5S_{1/2} \rightarrow 5D_{5/2}$ two-photon resonances. The optical frequency for the two-photon transitions is ~770 THz, an f_r harmonic on the order of 7.7×10^6. Therefore, the two-photon resonance condition is satisfied every time f_r is changed by ~13 Hz, corresponding to a change in the comb frequency by $f_r/2$ for the mode orders around 3.85×10^6. However, the data (Fig. 3) clearly show that the larger, one-photon resonantly enhanced peaks repeat after a change of f_r by ~26 Hz. As mentioned earlier, for the resonantly enhanced peaks, the pair of comb modes that is actually tuned onto the 5S-5P and 5P-5D resonances makes the dominant contribution to the two-photon transition rate.

The peak corresponding to nonresonant excitation of the $5S_{1/2}$ (F = 2) → $5P_{3/2}$ (F = 3) → $5D_{5/2}$ (F = 4) transition, made possible by the collective action of many comb modes, is larger than that theoretically predicted because the comb spectral phase is not flat and the comb spectrum is not symmetric around the P state; thus, the destructive interference mentioned earlier is reduced. Furthermore, as the detuning from the P state becomes greater than a few THz, the effect of phase mismatching between comb pairs over the spatial dimension of the MOT can be non-negligible.

DFCS enables us to measure all of the allowed single- and two-photon transitions within the laser bandwidth by a quick scan of f_r, thus eliminating the need for a broadly tunable and absolutely referenced cw laser. The two resonance peaks observed in the experimental spectrum that are not present in the theory model are due to the $5S_{1/2} \rightarrow 7S_{1/2}$ two-photon transition. For this f_r scan, the initial ground-state population is in F = 2. At longer times (blue curves), all the transitions starting on F = 2 are decreasing in amplitude compared to shorter time scales (red curves) due to ground-state population redistribution and heating. Most of the F = 1 peaks remain unchanged or become larger. Our density-matrix simulation accounts for the time dependence of the shutter response and optical pumping dynamics, but does not include any heating effects. The signal size shown in Fig. 3 has been normalized against the square of the probe power. Not surprisingly, both theory and experiment reveal that the most dominant transition pathway is $5S_{1/2}$ (F = 2) →

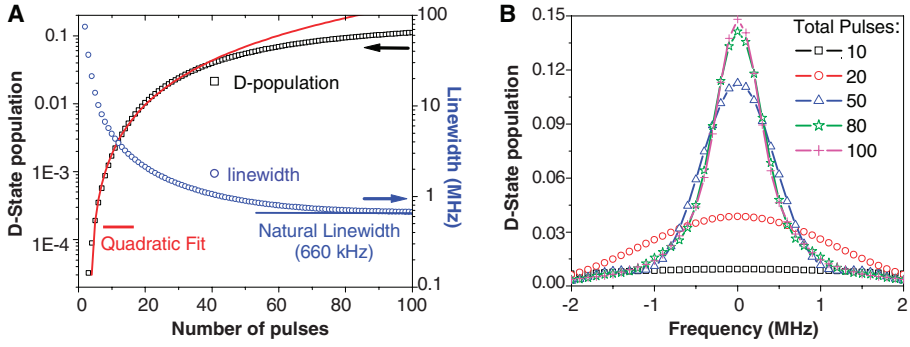

Fig. 2. (**A**) Left (right) axis shows calculated 5D population (linewidth) on resonance for the closed two-photon transition versus total number of accumulated pulses. The time between pulses is ~10 ns, and the system reaches its asymptotic values of signal amplitude and linewidth after ~480 ns. This theory plot illustrates that the DFCS resolution is limited only by the 5D natural linewidth. The quadratic fit to the 5D population at short times shows that the signal scales as the square of the number of pulses until atomic decoherence limits the coherent pulse accumulation. (**B**) The corresponding 5D resonance lineshape versus the number of pulses. In the first 10 pulses, the comb structure is not developed sufficiently to offer appreciable signal or resolution.

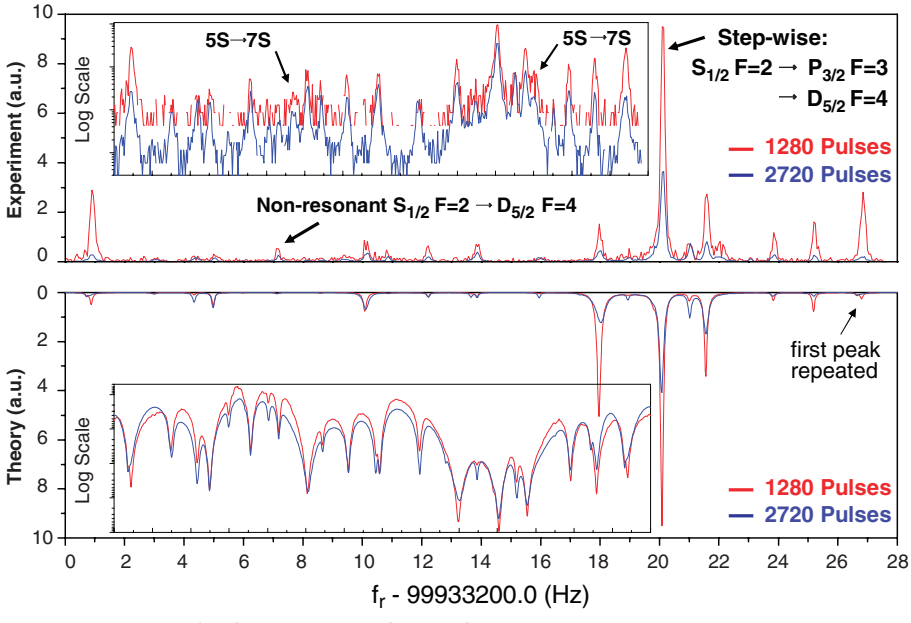

Fig. 3. Experimental (**top**) and simulated (**bottom**) two-photon spectra obtained with a frequency scan of f_r. Shifting f_r by 26 Hz shifts the comb spectrum by 100 MHz, or f_r, approximately repeating the original comb structure. The changes in relative peak sizes from the spectrum obtained after 1280 pulses (in red) to that after 2720 pulses (in blue) illustrate population transfer dynamics by optical pumping as well as heating effects. All 28 possible 5S → 5D two-photon transitions are observed, including resonantly enhanced and nonresonant cases. Two resonances in the data due to the 5S → 7S transition are not included in our model.

$5P_{3/2}$ (F = 3) → $5D_{5/2}$ (F = 4), which is the only closed transition.

The relative size of the features in Fig. 3 after any fixed number of pulses reflects intermediate-state resonant enhancement as well as population transfer. Thus, the spectrum contains all of the fine and hyperfine structure pertinent to the 5D states, while spectroscopy of the 5P states is performed via their resonant enhancement of the two-photon transition as a function of δ_{SP}. We defer further discussion of the P-state spectroscopy, however, until we have explored two important sources of possible systematic error: the mechanical action of the light on the atoms and AC Stark shifts.

Mechanical action of the probe. Although the sub-Doppler temperature established by polarization-gradient cooling provides an ideal initial condition for spectroscopy, it cannot be expected to survive the momentum transferred by the light from the comb. At best, the mean-square momentum will increase, leading to Doppler broadening. Worse, the momentum acquired may lead to systematic shifts in the resonance line positions. Thus, we seek to understand momentum transfer from the comb and to mitigate its effects insofar as possible.

We expect that the momentum transfer is dominated by the interaction of the comb mode closest to resonance with the 5S-5P transition, given that the radiative decay rate of the 5P-5S transition is an order of magnitude greater than that of 5D-5P, and the population largely resides in the 5S state. For ease of modeling, we used a single-beam (traveling wave) configuration and chose a comb structure such that the closed $5S_{1/2}$ (F = 2) → $5P_{3/2}$ (F = 3) → $5D_{5/2}$ (F = 4) transition is dominant. The temporal signal evolution is shown in Fig. 4 for the initial detunings of $\delta_{SP} = 0$ (○), $\delta_{SP} = 1$ MHz (▽), and $\delta_{SP} = 2$ MHz (◇). In the fully resonant case (○), the delayed signal peak at 30 μs reflects the switching time of our liquid crystal shutter. The subsequent decay arises as the accumulated momentum transfer gradually blue-shifts the atoms out of two-photon resonance. Although the 5S-5P transition controls the mechanical action, the two-photon resonance condition plays a more decisive role in the observed signal decay due to the 10-times-narrower D-state linewidth. When $\delta_{SP} = 1$ MHz (▽), the atoms, initially with $\delta_{SD} = 2$ MHz, will only reach the peak of the two-photon resonance after they have reached the velocity at which the Doppler shift compensates the initial detuning. Beyond this velocity, the signal contribution decreases. Similarly, when $\delta_{SP} = 2$ MHz (◇), the signal peaks still later.

All three experimental results agree well with our theory (solid lines in Fig. 4) based on a simple two-level dissipative light force model. The peak position is determined by the scattering rate, photon recoil, and the initial detunings. The width and shape of the peak are associated with the stochastic nature of radiation pressure, the intensity variation over the radial beam profile, and the finite laser linewidth. It is evident that the force exerted on an atom by the optical comb is well modeled by the radiation pressure due to a single comb mode tuned close to the 5S-5P resonance.

As a first step in mitigating the effect of light-induced momentum transfer, we used intensity-balanced counterpropagating beams. Even though the pulses do not overlap temporally inside the atomic cloud, they do interact with the same group of atoms within the atomic coherence time, leading to a

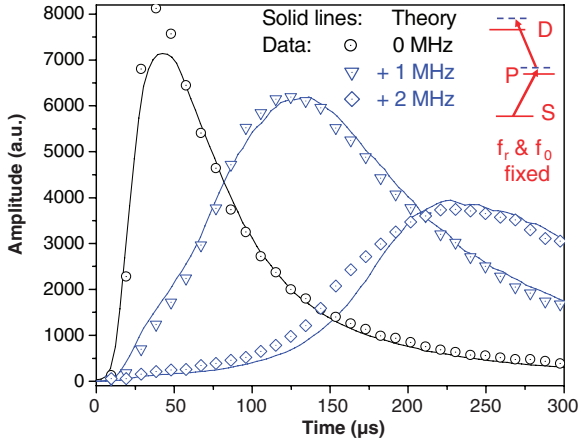

Fig. 4. Momentum transferred by the optical frequency comb (in a single probe beam configuration) to the cold Rb atoms, observed via the time-dependent fluorescence signal from the 5D states. The optical comb has fixed values of f_r and f_0 to achieve the desired detunings (with respect to atoms initially at rest) of $\delta_{SP} = \delta_{SD} = 0$ (black circles); $\delta_{SP} = 1$ MHz, $\delta_{SD} = 2$ MHz (blue triangles); and $\delta_{SP} = 2$ MHz, $\delta_{SD} = 4$ MHz (blue squares), respectively, for the dominant pair of comb modes.

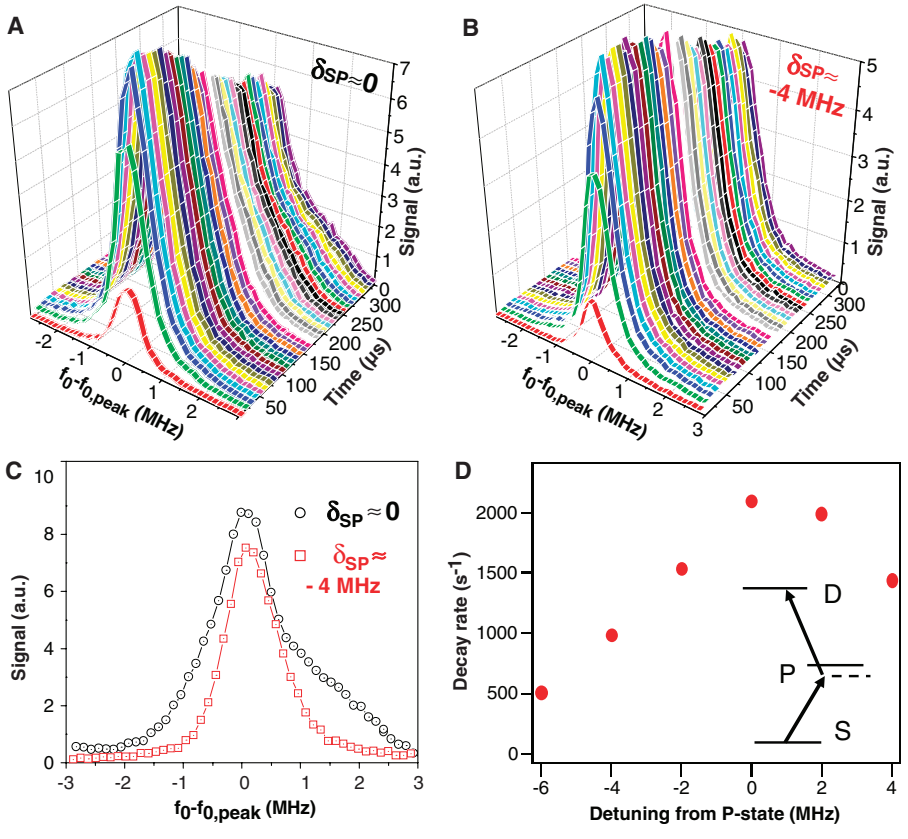

Fig. 5. Time evolution of the 5D fluorescence signal lineshape showing the mechanical action of the optical comb for the case of two balanced counterpropagating probe beams. f_r is fixed while f_0 is scanned over the 5D resonance profile. At the f_0 value corresponding to the expected line center, there are two cases of P-state detuning, (**A**) $\delta_{SP} \approx 0$ and (**B**) $\delta_{SP} \approx -4$ MHz. (**C**) A detailed comparison of the lineshape under the two detuning conditions after an interaction time of 300 μs. (**D**) The decay rate of the peak signal is reduced when the comb mode is tuned below, rather than on or above, 5S-5P resonance; thus, appropriately engineered comb modes can mechanically confine atoms for longer interrogation times.

signal enhancement by a factor of 4 compared to the single-beam case. Again we studied the momentum transfer associated with the $5S_{1/2}$ (F = 2) → $5P_{3/2}$ (F = 3) → $5D_{5/2}$ (F = 4) transition, fixing f_r and scanning f_0. Figure 5, A and B, show time evolutions of the detected signal as f_0 is swept, for two different detuning conditions: $\delta_{SP} = 0$ in Fig. 5A and $\delta_{SP} = -4$ MHz in Fig. 5B, when f_0 is tuned to the two-photon resonance peak. As f_0 is scanned to recover the resonance lineshape, the value of δ_{SP} changes. It is clear that the directed momentum transfer seen in Fig. 4 is greatly suppressed, and the heating is more evident. For the case of $\delta_{SP} \approx 0$, the lineshape profile centered at 300 μs (Fig. 5C, black circles) shows a marked asymmetry. This feature is easily understood, because the comb lines are tuned blue relative to both the 5S-5P and 5S-5D resonances, although the detuning of 5S-5P is less dramatic because its linewidth is an order of magnitude larger. Thus, Doppler heating accompanies the probe of the blue side of the two-photon resonance.

For the case of $\delta_{SP} \approx -4$ MHz, the intermediate-state detuning is always red as the two-photon resonance is probed. The red-detuned comb mode helps to maintain a symmetric absorption lineshape even after 300 μs, as confirmed by the corresponding profile (Fig. 5C, red squares). Thus, a judicious choice of comb structure can help to mitigate the heating of the sample caused by the probing beam. From Fig. 5, A and B, we also observe quite different signal decay rates versus observation time. A reduced signal decay rate attributed to less heating in the red-detuned case compared to the blue-detuned case is reflected in the asymmetric curve around $\delta_{SP} = 0$ (Fig. 5D).

AC Stark shift. Another systematic source of error is the light-induced AC-Stark shift on various atomic states to be measured. To assess this effect in the presence of many comb modes, we again took advantage of the flexibility in control of f_r and f_0 to vary δ_{SP} while keeping δ_{SD} nearly zero for the closed transition. In this near-resonance stepwise transition case, a nonvanishing value of δ_{SP} causes a shift in the measured two-photon transition frequency (*19*). To clearly distinguish the AC-Stark shift from mechanical actions, we gradually increased the power of the pulses as the laser shutter opened. For both $\delta_{SP} = +4$ MHz (△) and $\delta_{SP} = -4$ MHz (□) cases, the AC Stark shifts are present as soon as the laser is turned on and the transition frequency shift follows the time evolution of the peak power of the pulse train (Fig. 6A). When $\delta_{SP} = 0$ (○), the measured AC Stark shift is close to zero when the shutter just opens. The frequency shift measured at later times is attributed to the accumulated photon momentum transfer, which is reduced in the detuned cases. Again, the solid lines represent theoretical results obtained from a simple model of the AC-Stark shifts and mechanical action. The asymmetry in frequency shift between the red and blue detunings is caused by the presence of other 5P hyperfine states that also perturb the 5S-5D transition.

Although the laser spectrum spans roughly 26 THz, the obtained spectroscopic resolution approaches the atomic natural linewidth. This level of resolution is a result of the use of ultracold atoms and careful control of the phase-stabilized comb parameters, stray magnetic fields, light-induced shifts, and photon-momentum transfer. We typically measured two-photon linewidths on the order of 1 MHz, which is consistent with the convolution of the natural linewidth of 660 kHz and the laser technical linewidth of 300 kHz. The measured transition linewidth is slightly smaller for red detuning ($\delta_{SP} = -4$ MHz) than blue detuning (at the same $|\delta_{SP}|$ value) with the same probe power, again showing the benign effect of mechanical action by the red-detuned comb mode.

Absolute frequency measurement. With the understanding of systematic effects, we have analyzed spectra similar to the ones shown in Figs. 3 and 6A to construct a table of absolute transition frequencies from 5S to 5P and to 5D (Table 1). Some representative transition frequencies are determined directly from the comb structure and are given in the table, along with comparisons to available published values (*20*–*22*). Without any previous information of the 7S energy levels, we have also determined their absolute transition frequencies (*23*) by scanning the resonances for two sufficiently different values of f_r to determine the corresponding comb mode numbers. A single optical comb thus provides atomic structural information in the optical, terahertz, and radio-frequency spectral domains. The measurement accuracy is currently a few kHz to a few tens of kHz for the D states and on the order of 100 kHz for the P states, comparable to the highest resolution measurements made with cw lasers. To determine the absolute frequencies of the 5S-5P transition, we have scanned the P state directly, using a set of f_r and f_0 pairs that have a range of detunings from the P state, and are all two-photon resonant. Retrieving the actual P-state lineshape requires normalization based on our density matrix model to remove the optical pumping caused by varying detunings from other P states.

Implications and applications of DFCS. The resolution of DFCS can be improved by locking the femtosecond laser to a cavity that has been used to reduce the line-

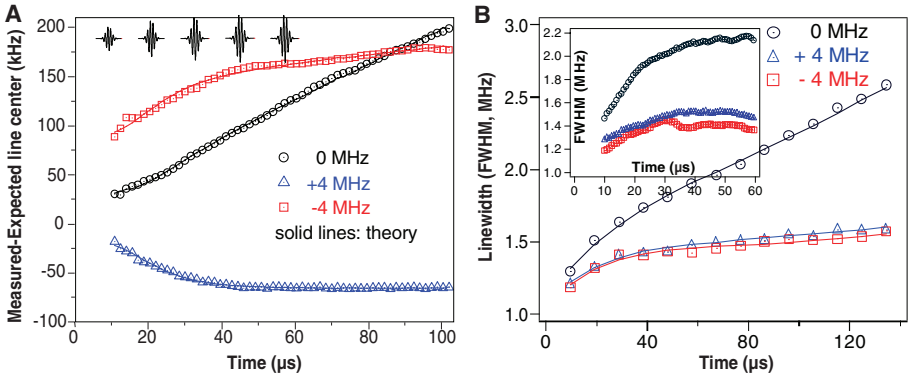

Fig. 6. Measurement of (**A**) the line center frequency and (**B**) linewidth for the closed two-photon transition, revealing frequency shifts from both the AC-Stark effect and mechanical action. Extrapolating to zero interrogation time and zero power yields the corrected atomic transition frequencies (A) and the natural transition linewidths (B).

Table 1. Rb level structure from direct frequency comb spectroscopy. All values are obtained by extrapolating the line-center to zero probing time and power.

Measured transition (from $5S_{1/2}$, F = 2)	Measured frequency (kHz)	Literature value (kHz)*
$5D_{5/2}$ F = 2	770,569,184,527.9 (49.3)	770,569,184,510.4 (16.0)
$5D_{5/2}$ F = 3	770,569,161,560.5 (11.1)	770,569,161,555.6 (16.0)
$5D_{5/2}$ F = 4	770,569,132,748.8 (16.8)	770,569,132,732.6 (16.0)
$5D_{3/2}$ F = 3	770,480,275,633.7 (12.7)	770,480,275,607.6 (10.0)
$5D_{3/2}$ F = 2	770,480,231,393.9 (38.1)	770,480,231,385.2 (10.0)
$5P_{3/2}$ F = 3	384,228,115,309.0 (63.0)	384,228,115,203.3 (7.1)
$5P_{1/2}$ F = 2	377,105,206,938.7 (179.0)	377,105,206,705.0 (400.0)

*From (*20*–*22*).

width to below 100 Hz (*24*). Similarly, a larger signal can be obtained by using a laser with a higher repetition rate; for example, a 1-GHz laser with the same average power and spectral width could increase the signal up to a 100-fold (*25*). One practical consequence of these results is a method to control both degrees of freedom of the femtosecond comb directly by an optical transition in cold atoms. Another interesting application of the demonstrated pulse accumulation effect is laser cooling of atoms that require coherent ultraviolet light not easily accessible by conventional laser sources (*26*). For general coherent control experiments, pulse accumulation (when enabled by long coherence times) can complement spectral amplitude and phase manipulations, leading to improved efficiency in population control with the added spectral resolution due to multipulse interference. The precise and phase-coherent pulse accumulation may prove particularly useful in efficiently populating atomic Rydberg states for quantum information processing. Although the current experiment involves two-photon transitions, the advantages of DFCS should apply equally to single-photon and multiphoton excitations. Multiple ultrafast lasers with optical spectra independently tailored for different spectroscopic features could be phase coherently stitched together (*27*, *28*) to further extend the utility of this approach.

References and Notes

1. T. C. Weinacht, J. Ahn, P. H. Bucksbaum, *Nature* **397**, 233 (1999).
2. A. H. Zewail, *Angew. Chem. Int. Ed.* **39**, 2587 (2000).
3. T. Udem, J. Reichert, R. Holzwarth, T. W. Hänsch, *Opt. Lett.* **24**, 881 (1999).
4. T. Udem, J. Reichert, R. Holzwarth, T. W. Hänsch, *Phys. Rev. Lett.* **82**, 3568 (1999).
5. L. S. Chen, J. Ye, *Chem. Phys. Lett.* **381**, 777 (2003).
6. S. A. Diddams *et al.*, *Science* **293**, 825 (2001).
7. J. Ye, L. S. Ma, J. L. Hall, *Phys. Rev. Lett.* **87**, 270801 (2001).
8. G. Wilpers *et al.*, *Phys. Rev. Lett.* **89**, 230801 (2002).
9. S. T. Cundiff, J. Ye, *Rev. Mod. Phys.* **75**, 325 (2003).
10. T. H. Yoon, A. Marian, J. L. Hall, J. Ye, *Phys. Rev. A.* **63**, 011402 (2000).
11. D. J. Jones *et al.*, *Science* **288**, 635 (2000).
12. N. Dudovich, B. Dayan, S. M. G. Faeder, Y. Silberberg, *Phys. Rev. Lett.* **86**, 47 (2001).
13. J. E. Bjorkholm, P. F. Liao, *Phys. Rev. Lett.* **33**, 128 (1974).
14. O. Poulsen, N. I. Winstrup, *Phys. Rev. Lett.* **47**, 1522 (1981).
15. R. Teets, J. Eckstein, T. W. Hänsch, *Phys. Rev. Lett.* **38**, 760 (1977).
16. M. J. Snadden, A. S. Bell, E. Riis, A. I. Ferguson, *Opt. Commun.* **125**, 70 (1996).
17. D. Felinto, C. A. C. Bosco, L. H. Acioli, S. S. Vianna, *Opt. Commun.* **215**, 69 (2003).
18. D. Felinto, L. H. Acioli, S. S. Vianna, *Phys. Rev. A.* **70**, 043403 (2004).
19. R. G. Brewer, E. L. Hahn, *Phys. Rev. A.* **11**, 1641 (1975).
20. F. Nez, F. Biraben, R. Felder, Y. Millerioux, *Opt. Commun.* **102**, 432 (1993).
21. J. Ye, S. Swartz, P. Jungner, J. L. Hall, *Opt. Lett.* **21**, 1280 (1996).
22. G. P. Barwood, P. Gill, W. R. C. Rowley, *Appl. Phys. B* **53**, 142 (1991).
23. A. Marian, M. C. Stowe, J. Ye, in preparation.
24. R. J. Jones, I. Thomann, J. Ye, *Phys. Rev. A.* **69**, 051803 (2004).
25. N. V. Vitanov, P. L. Knight, *Phys. Rev. A.* **52**, 2245 (1995).
26. D. Kielpinski, http://arxiv.org/abs/quant-ph/0306099 (2003).
27. R. K. Shelton *et al.*, *Science* **293**, 1286 (2001).
28. K. W. Holman, D. J. Jones, J. Ye, E. P. Ippen, *Opt. Lett.* **28**, 2405 (2003).

29. We are indebted to X.-Y. Xu, T. H. Yoon, L. S. Ma, T. M. Fortier, J. L. Hall, D. J. Jones, and E. Arimondo for their technical help and discussions during various stages of this work. The work at JILA is supported by the Office of Naval Research, NASA, NIST, and NSF.

24 September 2004; accepted 8 November 2004
Published online 18 November 2004;
10.1126/science.1105660
Include this information when citing this paper.

REPORTS

Building Programmable Jigsaw Puzzles with RNA

Arkadiusz Chworos,[1] Isil Severcan,[1] Alexey Y. Koyfman,[1,2] Patrick Weinkam,[1,4] Emin Oroudjev,[3] Helen G. Hansma,[3] Luc Jaeger[1,2]*

One challenge in supramolecular chemistry is the design of versatile, self-assembling building blocks to attain total control of arrangement of matter at a molecular level. We have achieved reliable prediction and design of the three-dimensional structure of artificial RNA building blocks to generate molecular jigsaw puzzle units called tectosquares. They can be programmed with control over their geometry, topology, directionality, and addressability to algorithmically self-assemble into a variety of complex nanoscopic fabrics with predefined periodic and aperiodic patterns and finite dimensions. This work emphasizes the modular and hierarchical characteristics of RNA by showing that small RNA structural motifs can code the precise topology of large molecular architectures. It demonstrates that fully addressable materials based on RNA can be synthesized and provides insights into self-assembly processes involving large populations of RNA molecules.

DNA has been extensively used to generate artificial geometrical objects like polyhedra (*1–3*), various self-assembling two-dimensional (2D) nanostructures (*1*, *4–6*), and DNA nanomechanical devices (*7–9*). Seeman, Winfree, and collaborators (*1*, *4*, *5*) have shown that DNA tiles based on various "crossover" DNA motifs could assemble in a predictable manner into periodic and aperiodic patterned 2D arrays. These DNA arrays are still made of a limited number of distinct molecular tiles and display rather simple patterning with no finite dimensions. However, their work suggests that versatile programmable molecular systems capable of algorithmic assembly into an infinite variety of 2D or three-dimensional (3D) supra-architectures with increasing pattern complexity, shape, molecular diversity, and size could potentially be generated with nucleic acids (*10*).

Although more chemically labile than DNA, natural RNAs offer a richer treasure trove of rigid structural motifs (*11–14*) that can be potential modules for supramolecular engineering (*15–20*). RNA tectonics (*15*) refers to the modular character of RNA, which can be decomposed and reassembled to create new RNA nanoscopic architectures. With the idea in mind to generate addressable materials with increasing patterns of complexity and molecular diversity, we have used a sequential stepwise assembly strategy to construct programmable building blocks with RNA tectonics. These molecules behave as "smart" RNA pieces, which could ultimately self-assemble in a predictable manner into any possible 2D architecture with full control over size, shape, and pattern geometry. Thus, the final position of each molecule can eventually be known and, therefore, be addressable, within a molecular jigsaw puzzle of finite size.

At a molecular level, "square-shaped" RNA supramolecules with sticky, interacting tails can potentially be programmed to assemble into many different planar networks of predefined geometries. We chose